Simple method for the simulation of multiple elastic scattering of electrons

D. Liljequist
University of Stockholm, Department of Physics, Vanadisv. 9, S-113 46 Stockholm, Sweden

F. Salvat, R. Mayol, and J. D. Martinez
Facultat de Fisica (ECM), Universitat de Barcelona, Diagonal 647, 08028 Barcelona, Spain

(Received 26 September 1988; accepted for publication 27 October 1988)

A screened Rutherford cross section is modified by means of a correction factor to obtain the proper transport cross section computed by partial-wave analysis. The correction factor is tabulated for electron energies in the range 0–100 keV and for elements in the range from $Z = 4$ to 82. The modified screened Rutherford cross section is shown to be useful as an approximation for the simulation of plural and multiple scattering. Its performance and limitations are exemplified for electrons scattered in Al and Au.

INTRODUCTION

To compute the plural or multiple elastic scattering in solids of electrons in the keV energy region one may use the accurate elastic differential cross section in a Monte Carlo code, which simulates multiple scattering as a succession of single events. This gives, in principle, a precise solution, provided that coherent (multiatom) scattering effects can be neglected. However, an accurate elastic differential cross section is obtained by means of a rather involved procedure. It has to be calculated, e.g., by means of partial-wave analysis (PWA) based on the Dirac equation, with an accurate scattering potential obtained from computed atomic wavefunctions. Moreover, the probability distribution for the scattering angle cannot be expressed in the closed form suitable for direct simulation by an inversion formula. An easily applied approximation of the PWA differential cross section may therefore be desirable.

To obtain an approximate cross section suitable for the plural and multiple scattering region, one may consider the autocorrelation length for the direction of motion of the electron, i.e., the transport mean free path λ_{tr}. The role of λ_{tr} as a quantity of primary importance for the electron transport has been discussed in a number of papers.[1–3] If the accurate differential elastic scattering cross section is to be approximated by another, simplified cross section, it is primarily required that they have the same λ_{tr} value.[1–3] Then, the two differential cross sections and their plural and multiple scattering angular distributions agree to first order when expanded in spherical harmonics.[4,5] The simplified cross section is then expected to be a good approximation provided that the scattering process considered is at least plural, i.e., the number of elastic collisions for the average trajectory should exceed a number of order of magnitude 10^1.[1]

We consider here elastic scattering only. The transport mean free path is

$$\lambda_{tr} = (N\sigma_{tr})^{-1}, \tag{1}$$

where N is the number of scatterers per unit volume and σ_{tr} the transport cross section,

$$\sigma_{tr} = \int_{-1}^{+1} \sigma(\cos\theta)(1-\cos\theta)d(\cos\theta), \tag{2}$$

where $\sigma(\cos\theta)$ is the elastic differential cross section in terms of scattering angle θ. The total cross section σ and elastic mean free path λ_e are

$$\sigma = \int_{-1}^{+1} \sigma(\cos\theta)d(\cos\theta), \tag{3}$$

$$\lambda_e = (N\sigma)^{-1}, \tag{4}$$

from which one has the relation

$$\lambda_{tr} = \lambda_e/(1-\langle\cos\theta\rangle), \tag{5}$$

where $\langle\cos\theta\rangle$ is the average value of $\cos\theta$ in a collision.

Where plural or multiple scattering is concerned, σ_{tr} rather than σ is the relevant quantity to consider. It is, therefore, of interest to study the dependence of σ_{tr} on the assumed atomic elastic scattering potential $V(r)$ and on the method of calculating the scattering cross section from this potential.

The atomic scattering potential adopted in the present work for the accurate (PWA) computation of σ_{tr} (cf. below) is obtained by means of atomic electron densities computed by the Dirac–Hartree–Fock–Slater (DHFS) self-consistent method under Wigner–Seitz (WS) boundary conditions.[6,7] This scattering potential is more accurate than other potentials (e.g., the DHFS potential for a free atom, the Thomas–Fermi–Dirac (TFD) potential, and analytic approximations[8,9] to these) that have been used as the basis for elastic multiple scattering calculations.

The scattering potential may be roughly approximated by the simple and well-known expression

$$V(r) = -(Ze^2/r)\exp(-r/R), \tag{6}$$

sometimes referred to as the Wentzel potential. The atomic screening radius R may be estimated by

$$R = a_0 Z^{-1/3} \tag{7}$$

where a_0 is the Bohr radius (0.529 Å). [Equation (7) differs slightly from the value estimated, e.g., by Ichimura *et al.*,[10,11] but this difference is not important in the present context.]

The Wentzel potential (6) is of practical interest, for the reason that the differential scattering cross section, computed in the first Born approximation, is extremely simple and convenient to apply in a simulation code. This fact has motivated its use in the method presented here.

 0021-8979/89/062431-08$02.40

MODIFIED SCREENED RUTHERFORD CROSS SECTION

Using the potential Eq. (6) and the first Born approximation, one obtains a screened Rutherford differential cross section

$$\sigma(\cos\theta) = \xi(1 - \cos\theta + \epsilon^{-1})^{-2}, \tag{8}$$

where

$$\xi = (\pi a_0^2/2)\left[4ZE + mc^2/E + 2mc^2\left(\frac{R_E}{E}\right)\right]^2. \tag{9}$$

Here, R_E is the Rydberg energy (13.606 eV), E the electron kinetic energy, and m the electron rest mass. The screening factor ϵ is given by

$$\epsilon = 2k^2R^2, \tag{10}$$

where k is the electron wave number. The total cross section is

$$\sigma = \xi[2\epsilon^2/(2\epsilon + 1)], \tag{11}$$

and the transport cross section is

$$\sigma_{tr} = \xi[\ln(2\epsilon + 1) - 2\epsilon/(2\epsilon + 1)]. \tag{12}$$

We shall by the notation SR refer to the screened Rutherford cross section, Eq. (8), with the screening radius R given by Eq. (7). Values of λ_{tr} obtained by means of Eq. (12) are exemplified in Table I. The values at the lowest energies are, for the heavy elements, clearly not reasonable; they are less than the size of the atom. This is due to the failure of the Born approximation.

In the context of plural and multiple scattering, the error of the SR cross section is primarily that it gives an incorrect transport mean free path. We therefore modify the SR cross section by introducing a correction factor

$$t_c = \lambda_{tr}/\lambda_{tr}(\mathrm{SR}) \equiv \sigma_{tr}(\mathrm{SR})/\sigma_{tr}, \tag{13}$$

where λ_{tr} is the accurate transport mean-free-path value, while $\lambda_{tr}(\mathrm{SR})$ is computed from the SR cross section [Eq. (12)]. The modified screened Rutherford (MSR) cross section is simply

$$\sigma_{\mathrm{MSR}}(\cos\theta) = t_c^{-1}\sigma_{\mathrm{SR}}(\cos\theta). \tag{14}$$

In practice, this correction means that the elastic mean free path λ_e is multiplied by t_c, i.e.,

$$\lambda_e(\mathrm{MSR}) = t_c\lambda_e(\mathrm{SR}). \tag{15}$$

The MSR cross section has the accurate values for σ_{tr} and λ_{tr}. It retains the screened Rutherford angular (θ) dependence, i.e.,

$$\sigma(\cos\theta) \propto (1 - \cos\theta + \epsilon^{-1})^{-2}, \tag{16}$$

which, depending on electron energy and atomic number, more or less well approximates the θ dependence of the accurate differential cross section.

One may note that the t_c factor accounts for two different corrections. The first one, which is the major one at lower energies, is the correction for the use of the first Born approximation instead of partial-wave analysis. The second one is the correction for the use of the potential in Eqs. (6) and (7) instead of an accurate scattering potential $V(r)$.

The correction of the SR cross section may be improved somewhat by modifying not only λ_e but also the screening factor ϵ. The requirement is then that not only the transport mean free path λ_{tr}, but also the elastic mean free path λ_e and the average scattering $\langle\cos\theta\rangle$ [cf. Eq. (5)] in a single collision should have the proper values. Under plural or multiple scattering conditions, the effect of this second correction is, however, small. Moreover, it turns out (cf. below) that the MSR cross section already has approximately the correct magnitude of λ_e except at very low energies.

TABLE I. Screened Rutherford (SR) transport mean free path (Å) for beryllium, aluminum, iron and gold.

Energy (eV)	Be	Al	Fe	Au
100	9.60(0)	3.01(0)	0.77(0)	0.25(0)
300	53.5 (0)	14.4 (0)	3.23(0)	0.81(0)
1000	41.0 (1)	10.0 (1)	20.8 (0)	4.40(0)
3000	28.6 (2)	66.0 (1)	13.2 (1)	25.6 (0)
10 000	25.1 (3)	55.9 (2)	10.9 (2)	20.0 (1)
30 000	18.4 (4)	40.1 (3)	76.8 (2)	13.6 (2)
100 000	15.5 (5)	33.2 (4)	62.7 (3)	10.9 (3)

NUMERICAL (PWA) COMPUTATION OF CROSS SECTIONS

Differential cross sections have been computed by solving the partial-wave expanded Dirac equation for the scattered electron wave function.[12] The scattering potential $V(r)$ has been obtained according to the usual static approximation, i.e., as the solution of Poisson's equation for the atomic charge distribution. The adopted atomic electron density has been determined following the relativistic DHFS self-consistent method.[6] In order to take some account of solid-state effects, the self-consistent calculations have been carried out under WS boundary conditions, that is, the atomic electrons are restricted to move within the WS sphere of radius $R_{\mathrm{WS}} = (3/4\pi N)^{1/3}$ and the radial derivative of the resulting atomic electron density vanishes at $r = R_{\mathrm{WS}}$.[7] As a consequence, the Coulomb field of the nucleus is completely screened outside the WS sphere, instead of being only exponentially screened as it is for free atoms. For atoms bound in solid phases, the use of the WS boundary conditions in the self-consistent computation directly leads to the (spherically averaged) static field $V(r)$, thus avoiding the use of additional approximations[13,14] to construct it from the free atom screened potential. Self-consistent atomic densities have been computed by using our own computer code.

A detailed description of numerical methods to compute the differential cross section has been given by Walker[12]; we shall mention here only the essential details of the present computation. The phase shifts have been evaluated numerically by solving the radial Dirac equations following Buring's power series method[12,15] after approximating the function $rV(r)$ by a cubic spline.[16] The grid of points in r is the same as that used in the self-consistent DHFS calculation (450 points logarithmically spaced in the interval from 0 to RWS) so that no additional interpolation errors are introduced by the spline approximation. The values of the phase shifts obtained in this way, being only affected by

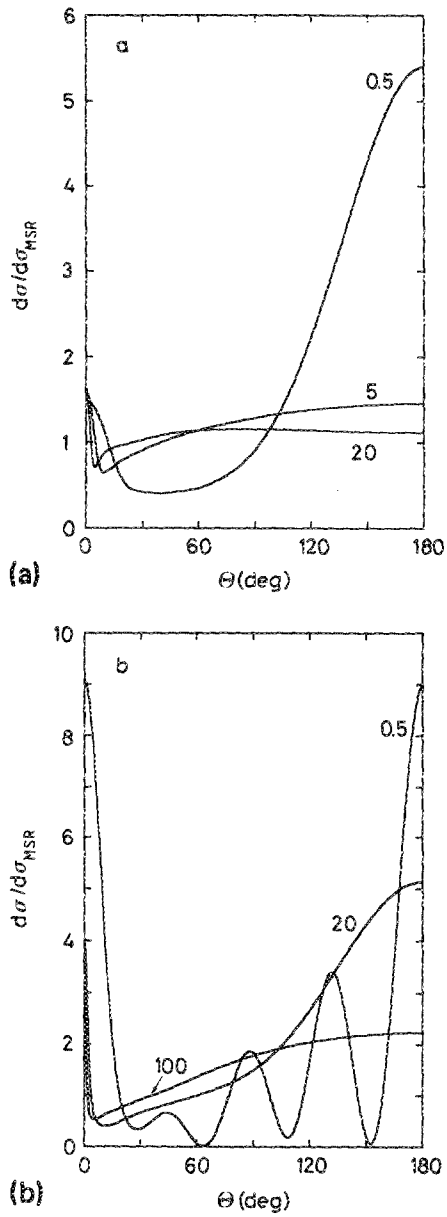

FIG. 1. Ratio of differential cross section computed by Dirac partial-wave analysis (DHFS scattering potential, WS boundary conditions) to the modified screened Rutherford (MSR) cross section for (a) aluminum at 0.5, 5, and 20 keV and (b) gold at electron energies 0.5, 20, and 100 keV.

round-off errors,[15] are expected to be highly accurate. The summation of the partial-wave series has been performed directly for scattering angles less than 2° and using the reduced series method of Yennie, Ravenhall, and Wilson[12] for scattering angles larger than this value. The number of computed phase shifts is large enough to ensure the convergence of the partial-wave series up to five decimal places.

Differential cross sections for electrons scattered by aluminum and gold are shown in Fig. 1. Actually, the plotted quantity is the ratio between the computed cross section and the modified screened Rutherford cross section [Eq. (14)]. It is worth mentioning here that this figure differs in detail from the results reported previously by Ichimura and coworkers[10,11]; the differences are due to the fact that neither the scattering potential[9] nor the screened Rutherford cross sections[17,18] used by those authors coincide with those adopted in the present work. To check this, we have performed a series of calculations for the TFD analytical scattering potential[9] used by Ichimura and co-workers and obtained results in excellent agreement with theirs.

It is interesting to analyze the effect of different scattering potentials on the computed cross sections. Total cross sections and transport cross sections computed from the DHFS static field for atoms in solids (WS atoms) and for free atoms are shown in Table II. The static field for free atoms has been obtained from the DHFS density computed under the usual (asymptotic) boundary conditions. For aluminum, it is seen that the cross sections for a free atom are larger than for a WS atom; this means that the atomic electron cloud is somewhat compressed in the solid (as compared with the free atom), thus having a more effective screening effect. For gold the situation is reversed; the cross sections for a WS atom are larger than for a free atom. The reason for this behavior lies in the high nuclear charge. The atomic electrons are tightly bound in a free gold atom, and the electronic cloud is slightly expanded when we require WS boundary conditions.

For comparison purposes, Table II also shows the cross sections obtained from the TFD analytical field[9] used in Refs. 10 and 11. It is seen that this potential leads to cross sections differing systematically from the DHFS ones. We have also included in this table the cross sections obtained from the WS scattering field by using the nonrelativistic partial-wave method (i.e., using the Schrödinger instead of the Dirac equation); the nonrelativistic results practically coincide with the corresponding relativistic data for small electron energies.

Table II also shows the total elastic cross section as computed from the MSR differential cross section. The values are, as mentioned previously, in rather good agreement with those obtained by partial-wave analysis for the WS atoms, except at the lowest energies. In fact, they are in many cases somewhat better than those obtained, e.g., by the TFD scattering potential.

For high-electron energies, the differential cross section takes its maximum value for forward scattering and decreases monotonously with increasing scattering angles. As small scattering angles correspond to large classical impact parameters, the differential cross section in this angular region is mainly determined by the details of the potential at large distances r from the nucleus. In fact, the scattering potentials for WS and free atoms practically coincide for small r values; they differ only at moderately large r. Hence, the WS and free atom differential cross sections are expected to differ essentially for small scattering angles. The main contribution to the total cross section is found at small scattering angles, so that the total cross section is quite sensitive to the details of the potential at large r. On the other hand, due to the weighting factor $[1-\cos(\theta)]$, the main contributions to the transport cross section come from intermediate and large scattering angles (irrespective of the electron energy) and, therefore, the transport cross section is rather independent of the particular scattering potential used.

TABLE II. Total elastic cross section σ and transport cross section σ_{tr} (in units of a_0^2) for aluminum and gold. Values in different columns have been computed from different scattering potentials, using different methods of calculation. WS atom: DHFS-WS scattering potential using Dirac partial-wave analysis (PWA); free atom: DHFS potential for free atoms using Dirac PWA; non-rel: the DHFS-WS potential using Schrödinger PWA; TFD atom: TFD analytical potential (Ref. 9) using Dirac PWA; MSR: modified screened Rutherford, Eqs. (11) and (14).

Element	Energy (keV)	WS atom	Free atom	Non-rel.	TFD atom	MSR
Al (13)	0.10	9.98(0)	1.66(1)	1.00(1)	7.09(0)	1.40(1)
(σ)	0.50	4.51(0)	6.61(0)	4.51(0)	5.62(0)	5.89(0)
	1.00	2.90(0)	4.10(0)	2.90(0)	3.61(0)	3.53(0)
	5.00	8.64(−1)	1.16(0)	8.53(−1)	1.07(0)	8.99(−1)
	10.00	4.73(−1)	6.28(−1)	4.61(−1)	5.84(−1)	4.74(−1)
	50.00	1.13(−1)	1.49(−1)	9.87(−2)	1.40(−1)	1.09(−1)
	100.00	6.48(−2)	8.52(−2)	4.97(−2)	7.98(−2)	6.15(−2)
Au (79)	0.10	2.21(1)	2.15(1)	2.03(1)	3.56(1)	6.78(0)
(σ)	0.50	1.11(1)	1.09(1)	1.10(1)	1.55(1)	8.75(0)
	1.00	8.28(0)	8.13(0)	8.25(0)	1.11(1)	9.32(0)
	5.00	3.96(0)	3.89(0)	3.92(0)	5.12(0)	4.79(0)
	10.00	2.76(0)	2.71(0)	2.71(0)	3.51(0)	3.13(0)
	50.00	1.09(0)	1.07(0)	9.84(−1)	1.34(0)	1.08(0)
	100.00	7.19(−1)	7.09(−1)	5.84(−1)	8.82(−1)	6.92(−1)
Al (13)	0.10	6.27(0)	6.70(0)	6.28(0)	1.24(1)	
(σ_{tr})	0.50	1.08(0)	1.09(0)	1.08(0)	1.13(0)	
	1.00	4.07(−1)	4.10(−1)	4.05(−1)	4.19(−1)	
	5.00	3.11(−2)	3.12(−2)	3.06(−2)	3.16(−2)	
	10.00	9.37(−3)	9.41(−3)	9.14(−3)	9.50(−3)	
	50.00	5.42(−4)	5.44(−4)	4.95(−4)	5.47(−4)	
	100.00	1.62(−4)	1.62(−4)	1.38(−4)	1.63(−4)	
Au (79)	0.10	4.69(0)	4.36(0)	4.77(0)	8.13(0)	
(σ_{tr})	0.50	3.22(0)	3.16(0)	3.46(0)	3.87(0)	
	1.00	2.34(0)	2.33(0)	2.43(0)	2.58(0)	
	5.00	4.12(−1)	4.12(−1)	4.02(−1)	4.26(−1)	
	10.00	1.60(−1)	1.60(−1)	1.50(−1)	1.64(−1)	
	50.00	1.47(−2)	1.47(−2)	1.20(−2)	1.51(−1)	
	100.00	5.11(−3)	5.11(−3)	3.71(−3)	5.22(−3)	

TABLE III. Correction factor t_c computed by Dirac PWA from DHFS-WS scattering potentials. For carbon, copper, and lead, see Table IV.

Energy (keV)	Element (atomic number)											
	Be(4)	Al(13)	Ca(20)	Fe(26)	Ge(32)	Sr(38)	Ag(47)	Sn(50)	Ba(56)	Gd(64)	W(74)	Au(79)
0.10	1.257	3.140	3.905	7.061	13.213	16.187	16.265	14.330	15.970	25.349	43.544	52.567
0.15	1.211	2.589	3.192	5.076	8.783	9.955	13.220	13.534	13.946	25.137	47.121	58.958
0.20	1.188	2.301	2.823	4.102	6.638	7.475	9.985	10.829	11.072	19.078	37.079	46.173
0.30	1.165	1.993	2.429	3.207	4.674	5.351	6.781	7.385	7.779	11.778	21.021	24.508
0.40	1.153	1.824	2.211	2.786	3.796	4.378	5.391	5.802	6.189	8.611	13.996	15.831
0.50	1.147	1.714	2.065	2.536	3.309	3.813	4.624	4.936	5.285	6.957	10.545	11.792
0.70	1.139	1.576	1.878	2.240	2.781	3.176	3.785	4.005	4.293	5.298	7.322	8.101
1.00	1.134	1.458	1.713	1.997	2.390	2.694	3.156	3.319	3.554	4.190	5.369	5.870
1.50	1.129	1.352	1.558	1.781	2.068	2.297	2.643	2.763	2.951	3.367	4.072	4.388
2.00	1.127	1.294	1.466	1.655	1.891	2.081	2.365	2.464	2.624	2.946	3.464	3.700
3.00	1.123	1.230	1.358	1.508	1.691	1.838	2.057	2.132	2.259	2.493	2.849	3.015
4.00	1.121	1.196	1.295	1.421	1.575	1.698	1.882	1.944	2.052	2.242	2.524	2.655
5.00	1.119	1.175	1.254	1.363	1.497	1.605	1.765	1.820	1.913	2.077	2.315	2.426
7.00	1.116	1.150	1.202	1.288	1.397	1.484	1.615	1.659	1.735	1.866	2.053	2.140
10.00	1.113	1.132	1.161	1.225	1.310	1.379	1.483	1.518	1.579	1.682	1.828	1.896
15.00	1.111	1.118	1.128	1.170	1.232	1.282	1.360	1.387	1.433	1.512	1.622	1.674
20.00	1.110	1.111	1.111	1.141	1.189	1.227	1.289	1.310	1.347	1.411	1.501	1.543
30.00	1.110	1.105	1.094	1.111	1.144	1.167	1.207	1.222	1.247	1.293	1.358	1.389
40.00	1.110	1.103	1.087	1.097	1.120	1.134	1.162	1.172	1.189	1.224	1.274	1.298
50.00	1.112	1.103	1.084	1.088	1.106	1.114	1.133	1.140	1.151	1.178	1.218	1.236
70.00	1.115	1.104	1.081	1.080	1.090	1.091	1.098	1.101	1.105	1.120	1.145	1.157
100.00	1.119	1.107	1.081	1.076	1.080	1.075	1.071	1.071	1.068	1.073	1.085	1.090

These features are clearly evidenced in Table II.

As multiple elastic scattering is mainly determined by the transport cross section, it follows that the results of Monte Carlo simulations of such processes will not depend strongly on the adopted scattering potential (provided that the differential cross sections are evaluated according to the relativistic partial-wave method).

COMPUTATION OF CORRECTION FACTOR t_c

Differential cross sections and transport cross sections for WS atoms have been computed for 15 elements and a grid of energies sweeping the periodic system and the energy range from 100 eV to 100 keV. The corresponding t_c correction, i.e., the ratio between the relativistic SR transport cross section and the transport cross section computed by partial-wave analysis as described above [Eq. (13)], is shown in Table III for 12 of these elements. Accurate values of the t_c correction for the elements considered at energies different from those included in Table III can be obtained by natural cubic spline interpolation[16] on the energy axis or, somewhat less accurately, by simple linear interpolation. As the energy grid points are nearly logarithmically spaced, it is convenient to use $\log(E)$ rather than E as an independent variable.

The t_c correction for elements not included in Table III can be evaluated approximately by spline interpolation on the atomic number (Z) axis. In order to investigate the accuracy of this interpolation, we have also computed the differential cross sections for carbon, copper, and lead and the corresponding t_c correction. The computed t_c values and the results of the natural spline interpolation on the Z axis, using the data in Table III, are compared in Table IV. The case of Pb shows in fact that even a moderate extrapolation may work satisfactorily. Of course, the three elements in Table IV can be used to complete Table III.

TABLE IV. Correction factor t_c for carbon, copper, and lead computed from the DHFS-WS scattering potential by Dirac PWA (calc.), and obtained from the values in Table III by natural cubic spline interpolation (int.).

Energy (keV)	C(6)		Cu(29)		Pb(82)	
	Calc.	Int.	Calc.	Int.	Calc.	Int.
0.10	1.506	1.773	10.154	10.181	43.737	57.926
0.15	1.394	1.574	7.184	7.039	52.101	66.080
0.20	1.330	1.473	5.521	5.433	45.521	51.584
0.30	1.257	1.370	3.987	3.958	25.950	26.488
0.40	1.217	1.316	3.310	3.295	16.794	16.855
0.50	1.192	1.282	2.933	2.923	12.472	12.491
0.70	1.163	1.240	2.517	2.510	8.537	8.547
1.00	1.140	1.207	2.199	2.193	6.160	6.162
1.50	1.123	1.177	1.929	1.925	4.576	4.574
2.00	1.115	1.161	1.777	1.773	3.843	3.839
3.00	1.107	1.144	1.603	1.600	3.115	3.113
4.00	1.103	1.135	1.501	1.499	2.735	2.733
5.00	1.100	1.129	1.433	1.431	2.493	2.492
7.00	1.097	1.122	1.344	1.343	2.193	2.192
10.00	1.095	1.117	1.269	1.268	1.938	1.936
15.00	1.093	1.113	1.202	1.201	1.705	1.705
20.00	1.093	1.111	1.166	1.165	1.568	1.568
30.00	1.093	1.110	1.129	1.128	1.407	1.407
40.00	1.094	1.110	1.110	1.109	1.312	1.312
50.00	1.096	1.111	1.098	1.097	1.247	1.247
70.00	1.099	1.114	1.087	1.085	1.164	1.164
100.00	1.104	1.118	1.079	1.078	1.093	1.093

PERFORMANCE

In order to demonstrate the performance and limitations of the method, Monte Carlo simulations using the modified screened Rutherford (MSR) cross section are compared with simulations using the accurate (PWA) differential cross section, i.e., the one used to compute the t_c values in Table III. We also compare with simulations using the original screened Rutherford (SR) cross section.

In all three cases we have, for simplicity, used the continuous slowing-down approximation, employing the stopping power formula due to Rao-Sahib and Wittry,[19] as it is a very simple, reasonably realistic extrapolation of the Bethe–Bloch formula down to low energies. It should be noted that the purpose here is to compare the results for the three different elastic cross sections with each other. We do not compare with the experiment as we have neglected a number of factors: (a) the error in the Rao-Sahib and Wittry stopping power, (b) the effect of straggling, (c) inelastic scattering, i.e., the contribution to σ_w from the inelastic events, and (d) secondary electron contributions.

The recipe for using the MSR cross section may be stated briefly: (1) Compute the SR mean free path $\lambda_e(\mathrm{SR})$ according to Eqs. (11) and (4). (2) Multiply by t_c [Eq. (15)], taking the t_c value by interpolation from Table III. This gives the elastic mean free path $\lambda_e(\mathrm{MSR})$ to be used in the simulation. (3) In the Monte Carlo program, simulate the scattering angle θ in an elastic event in accordance with the angular distribution of Eq. (16), e.g., by the FORTRAN statement,

$$CT = 1.0 + (Y - 1.0)/(EPS*Y + 0.5),$$

where $CT = \cos\theta$, $EPS = \epsilon$ as calculated by Eqs. (10) and (7), and Y is the standard pseudorandom number ($0 < Y < 1$). For rapid simulation, $\lambda_e(\mathrm{MSR})$ and ϵ are conveniently precalculated for a number of electron energy channels.

The PWA simulations presented here have been performed by means of numerical differential cross sections, which are introduced in the simulation program as data for a grid of points (E_i, θ_j) (= energies, angles) dense enough and conveniently distributed to allow accurate interpolation. The total cross section is evaluated by cubic spline interpolation on the energy axis. The scattering angle for a given energy is directly given by the inverse cumulative distribution function with a standard pseudorandom number as argument; however, this function is only known for the energies E_i in the grid. To sample the scattering angle for a given energy, a single value of the pseudorandom number is generated and used to obtain the scattering angle for the two nearest energies in the grid. The resultant scattering angle is obtained by linear interpolation.

We compare SR, MSR, and PWA results for collimated electron beams normally incident on aluminum and gold foils, representing low- and high-Z materials, respectively. The angular distribution of transmitted low-energy elec-

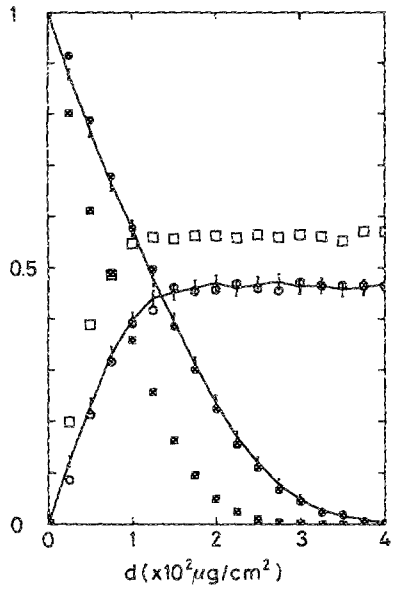

FIG. 2. Transmission and backscattering of 10 keV electrons normally incident on gold foils of thickness d. Error bars joined by curves show the results using the PWA differential cross section. Filled and open circles show the result for transmission and backscattering, respectively, using the modified screened Rutherford (MSR) cross section, while filled and open squares show the result using the original screened Rutherford (SR) cross section.

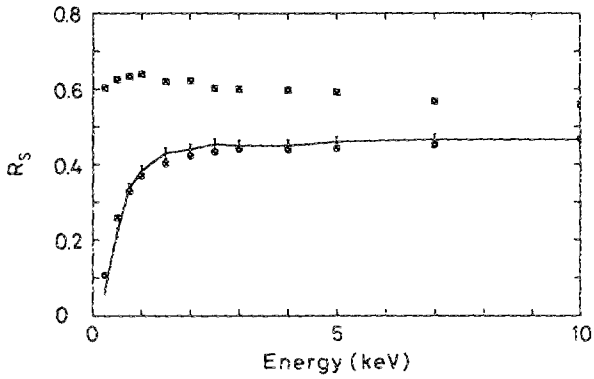

FIG. 4. Energy dependence of the bulk backscattering fraction R_s of gold, simulated using the PWA differential cross section (error bars joined by curve), the modified screened Rutherford (MSR) cross section (filled circles), and the original screened Rutherford (SR) cross section (filled squares).

trons incident on high-Z thin foils represents a "worst" case as regards to the applicability of the MSR cross section, and is, therefore, considered in some detail.

Comparison of simulated total transmission and backscattering for electrons incident on Au and Al foils are shown in Figs. 2 and 3. The effect of the correction factor t_c is considerable in the case of 10 keV electrons incident on Au (Fig. 2). The agreement between data simulated by the accurate (PWA) cross section and the MSR cross section is good. The MSR simulation gives a slightly too low backscattering at the smallest thicknesses, due to near single scattering conditions and the large difference between the PWA and MSR differential cross sections at low energies in gold [cf. Fig. 1(b)]. For $\simeq$20 keV electrons scattered in aluminum, the correction factor is rather near unity (Table III), so the effect of the correction, though adequate, is small (Fig. 3).

Figure 4 shows the effect of the correction factor t_c in the simulation of the bulk backscattering fraction of gold (normal incidence) at different electron energies. The characteristic decrease of the bulk backscattering fraction R_s at low energies is well known from previous experimental and theoretical work.[20] The results using the MSR and PWA cross sections are in good agreement.

Transmission and backscattering are less sensitive to the shape of the differential cross section than angular distributions (cf. below), and one gets good results using the MSR down to quite small foil thicknesses. In fact, enforcing the

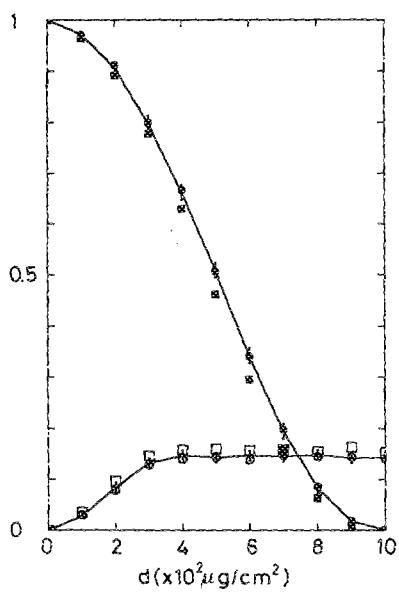

FIG. 3. Transmission and backscattering of 20 keV electrons normally incident on aluminum foils of thickness d. Notations are the same as in Fig. 2.

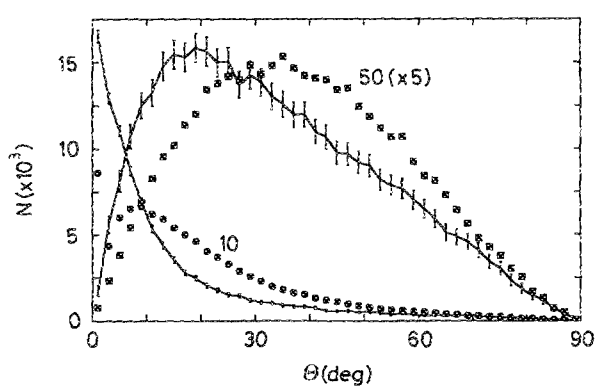

FIG. 5. Angular distributions of 10 keV electrons transmitted through gold foils of thickness 10 and 50 μg/cm^2. Error bars (curves) show results using the PWA differential cross section, while circles and squares show the results using the MSR differential cross section. Vertical axis shows the number of electrons recorded in respective angular channels. For the thinner foil thickness, the most probable scattering angle using the PWA cross section is not resolved at the angular resolution used in the figure.

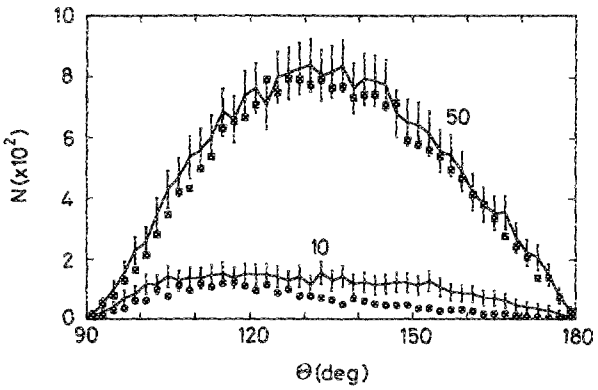

FIG. 6. Angular distributions of 10 keV electrons backscattered from gold foils of thickness 10 and 50 μg/cm^2 simulated by means of PWA and MSR differential cross sections. Notations are the same as in Fig. 5.

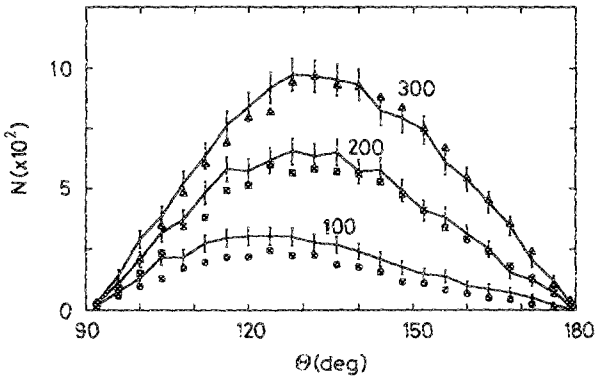

FIG. 8. Angular distributions (PWA and MSR) of 30 keV electrons backscattered from gold foils of thickness 100, 200, and 300 μg/cm^2. Notations are the same as in Fig. 7.

correct transport mean free path, one gets good agreement with the PWA and MSR transmission and backscattering (Figs. 2–4) even when using extremely simplified scattering models, such as, e.g., a fixed scattering angle in each collision.[1–3] It has also been shown that the variation of bulk backscattering with varying angles of incidence is well reproduced with such scattering models.[2] Figures 2–4 confirm that analysis in terms of the transport mean free path should be useful for the understanding of total transmission and backscattering, as suggested previously.[2]

Figures 5 and 6 compare angular distributions obtained with the PWA and MSR cross sections for 10 keV electrons transmitted and backscattered in rather thin foils of gold. The MSR approximation is rough in particular for the angular distribution transmitted through the thinnest layer (10 μg/cm^2). In order for the approximation method to be generally good, the scattering process should involve a sufficient number of collisions; as an estimate, d/λ_e should exceed a number of order of magnitude 10^1.[1] Using the MSR value for λ_e, the gold foil thicknesses 10 and 50 μg/cm^2 correspond to $d/\lambda_e \approx 3$ and $d/\lambda_e \approx 14$, respectively. The difference between the PWA and MSR angular distributions in this case again reflects the considerable difference between the corresponding single scattering angular distributions [cf., Fig. 1(b)]. Backscattering angular distributions are, however, rather well simulated with the MSR cross section except for very thin layers (Fig. 6).

Further examples for the case of gold are shown in Figs. 7 and 8, for 30 keV electrons normally incident on foils of thicknesses of 100, 200, and 300 μg/cm^2. The total transmission as simulated by MSR is 0.94, 0.84, and 0.75, respectively. The d/λ_e values are ≈ 13, 26, and 40, respectively. The simulated PWA and MSR angular distributions of transmitted electrons show a slow convergence towards better agreement (Fig. 7). For the backscattered angular distributions the agreement is good except that the total backscattering with the MSR cross section is somewhat too low for the thinnest layers (Fig. 8).

The case of 20 keV electrons incident on aluminum foils of thicknesses of 100, 200, and 300 μg/cm^2 is, likewise, in the transition region to multiple scattering ($d/\lambda_e \approx 16$ for 100 μg/cm^2). The PWA and MSR cross sections are fairly similar [Fig. 1(a)], so a rapid convergence between PWA and MSR angular distributions with an increasing number of collisions is expected. This is confirmed by Figs. 9 and 10.

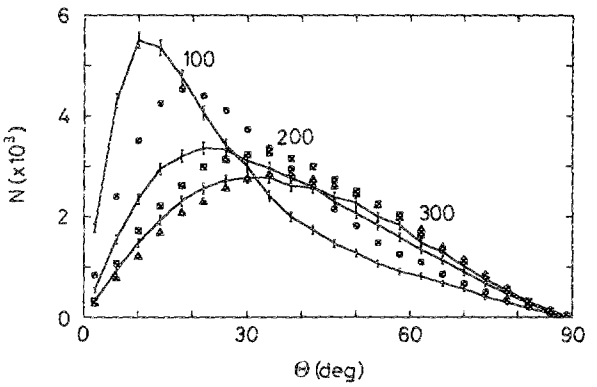

FIG. 7. Angular distributions of 30 keV electrons transmitted through gold foils of thickness 100, 200, and 300 μg/cm^2 simulated by means of PWA and MSR differential cross sections. Notations are similar to those in Fig. 5; filled triangles show the MSR result for $d = 300$ μg/cm^2.

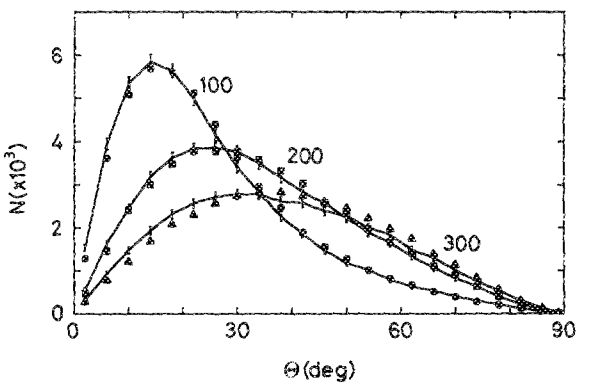

FIG. 9. Angular distributions (PWA and MSR) of 20 keV electrons transmitted through aluminum foils of thickness 100, 200, and 300 μg/cm^2. Notations are similar to those in Figs. 7 and 8.

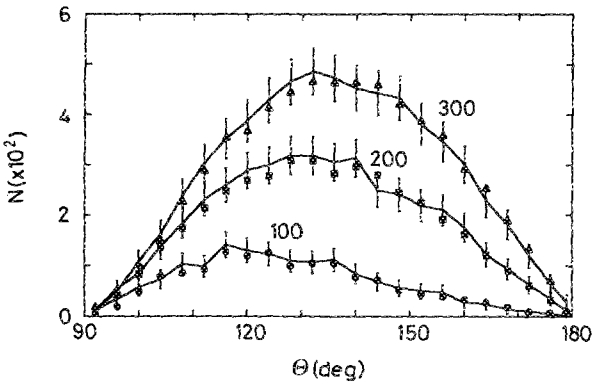

FIG. 10. Angular distributions (PWA and MSR) of 20 keV electrons backscattered from aluminum foils of thickness 100, 200, and 300 $\mu g/cm^2$. Notations are similar to those in Figs. 7 and 8.

We refrain from comparing energy loss distributions, since we have not included a realistic straggling model. Previous results with simplified elastic scattering cross sections[1,2,21] indicate, however, that the MSR should be useful for this purpose.

SUMMARY

A method has been presented, where the elastic scattering as computed by the procedure of partial-wave analysis for an accurate atomic scattering potential is taken approximately into account by correcting a simple screened Rutherford cross section. The correction factor t_c has been tabulated for the low and intermediate electron energy region ($\sim 10^{-1} - 10^2$ keV).

At higher energies (towards 100 keV and above) the method has to be modified since the direct simulation of elastic events is not practical with the large number of collisions involved. The modification can be made by enforcing the proper transport cross section on a suitably simplified cross section using an artificially enlarged mean free path.[3] We are presently considering the computation of the corresponding t_c factor for high electron energies.

ACKNOWLEDGMENTS

This work has been partially supported by the Comision Interministerial de Ciencia y Tecnologia (Spain), Contract No. PB86-0589. One of the authors (F.S.) also wishes to thank the Consejo Superior de Investigaciones Cientificas for a Travel Grant.

[1] D. Liljequist, J. Appl. Phys. **62**, 333 (1987).
[2] D. Liljequist, J. Phys. D **10**, 839 (1978).
[3] D. Liljequist and M. Ismail, J. Appl. Phys. **62**, 342 (1987).
[4] S. Goudsmit and J. L. Saundersson, Phys. Rev. **57**, 24 (1940).
[5] H. W. Lewis, Phys. Rev. **78**, 526 (1950).
[6] D. A. Liberman, J. T. Waber, and D. T. Cromer, Phys. Rev. **137**, A27 (1965); D. A. Liberman, D T. Cromer, and J. T. Waber, Comput. Phys. Commun. **2**, 107 (1971).
[7] R. Mayol, J. D. Martinez, F. Salvat, and J. Parellada, Ann. Fis. A 80, **130** (1984).
[8] F. Salvat, J. D. Martinez, R. Mayol, and J. Parellada, Phys. Rev. A **36**, 467 (1987).
[9] R. A. Bonham and T. G. Strand, J. Chem. Phys. **39**, 2200 (1963).
[10] S. Ichimura, M. Aratama, and R. Shimizu, J. Appl. Phys. **51**, 2853 (1981).
[11] S. Ichimura and R. Shimizu, Surf. Sci. **112**, 386 (1981).
[12] D. W. Walker, Adv. Phys. **20**, 257 (1971).
[13] A. J. Green and R. C. G. Leckey, J. Phys. D **9**, 2123 (1976).
[14] M. Kotera, K. Murata, and K. Nagami, J. Appl. Phys. **52**, 7403 (1981).
[15] W. Buhring, Z. Phys. **187**, 180 (1968).
[16] M. J. Maron, *Numerical Analysis: A Practical Approach* (Macmillan, New York, 1982).
[17] T. Matsukawa, K. Murata, and R. Shimizu, Phys. Status Solidi B **55**, 371 (1973).
[18] B. P. Nigam, M. K. Sundaresan, and Ta-Yau Wu, Phys. Rev. **115**, 491 (1959).
[19] T. S. Rao-Sahib and D. B. Wittry, J. Appl. Phys. **45**, 5060 (1974).
[20] M. Kotera, K. Murata, and K. Nagami, J. Appl. Phys. **52**, 997 (1981).
[21] D. Liljequist, J. Appl. Phys. **57**, 657 (1985).